Symmetry breaking of a parallel two-phase flow in a finite length channel

Paul R. Kaneelil [1], Amir A. Pahlavan [1,2], Miguel A. Herrada [3], Kristen LeRoy,[4]
Kylie Stengel,[4] Samuel Warner [4], Anna M. Galea,[4] and Howard A. Stone [1,*]

[1]*Department of Mechanical and Aerospace Engineering, Princeton University,
Princeton, New Jersey 08544, USA*
[2]*Department of Mechanical Engineering and Material Science, Yale University,
New Haven, Connecticut 06511, USA*
[3]*Departamento de Mecánica de Fluidos e Ingeniería Aeroespacial,
Universidad de Sevilla, Seville 41092, Spain*
[4]*Lung Biotechnology PBC, Sudbury, Massachusetts 01776, USA*

Parallel two-phase flows are omnipresent in technological applications that require
contact between two immiscible fluids for a finite amount of time. Precise control over
the flow and separation of the fluids once they have been in contact are therefore the
key challenges in these applications. Here, using experiments and numerical simulations,
we show that the interface between two immiscible fluids flowing at the same flow rate
in a symmetric channel can become unstable locally near the exit junction, where the
two fluids are separated. This instability leads to the shedding of the droplets of one
phase into the other, preventing a complete separation. We characterize this instability
and show that the period of drop shedding is inversely proportional to the flow rate. We
derive a stability criterion based on the balance between the Laplace pressure across the
liquid-liquid interface and viscous pressure drop along each flow stream. The stability
criterion and our experimental results are used to highlight the extreme sensitivity of this
flow system to the parameters involved such as viscosity difference and exit geometry,
which introduces gravitational effects and characteristics of the exit tubing.

I. INTRODUCTION

Laminar, parallel two-phase fluid flows often refer to immiscible fluids flowing side-by-side in microchannels and are common in many applications involving chemical reactions [1–5], mass transfer, and separations [6–9]. While the conditions for stability of parallel flows in infinitely long channels are well established [10–12], much less is known about the stability of flow in finite channels that are relevant to applications.

In finite channels, the two immiscible fluids are brought into contact at an inlet junction, flow side by side over a certain length, and are then separated downstream at an exit junction (Fig. 1). Earlier studies have reported that the separation is typically imperfect, leading to the undesirable leakage of one of the streams into the exit of the other. These works have attributed the imperfect separation to the mismatch between the viscous pressure drop along the streams versus the Laplace pressure jump across the interface and have proposed different strategies to achieve complete separation [1,13–17]. Although several mitigation strategies have been proposed to stabilize the

---

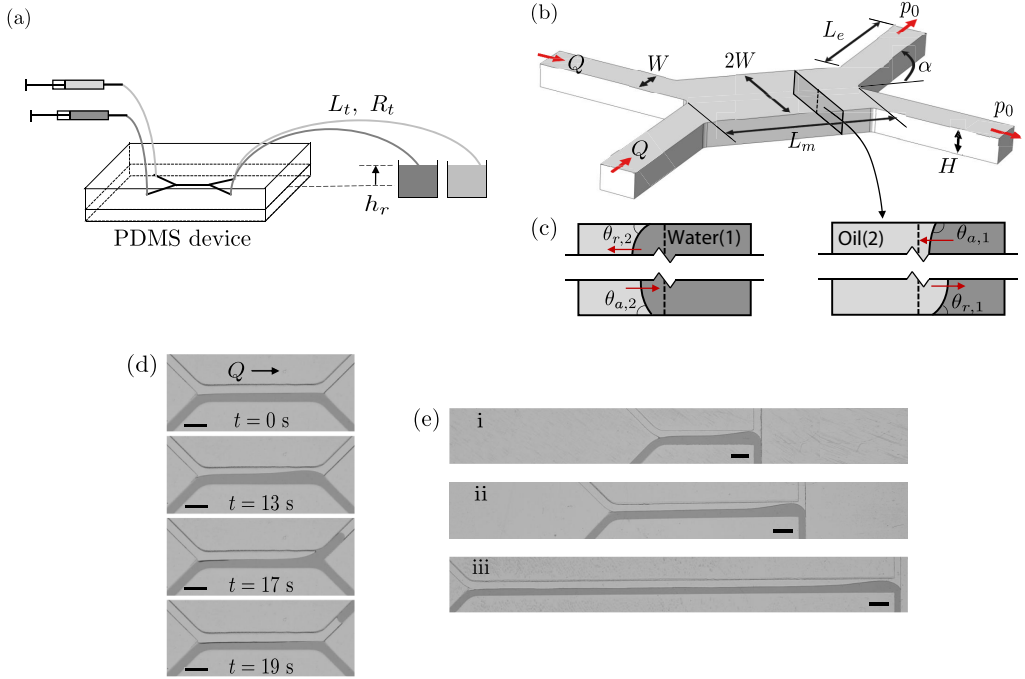*Corresponding author: hastone@princeton.edu

FIG. 1. The experimental setup and the instability. (a) Schematic showing the flow system: we inject the two immiscible liquids via the two inlets at equal flow rates Q, and the outlets drain into respective fluid reservoirs where the exit pressure is p_0 (atmospheric pressure). PTFE tubes of length L_t and radius R_t carry the liquids from the syringes to the inlet and from the exit to their respective reservoirs. (b) 3D schematic of the channel showing the various geometric parameters. (c) Schematics showing the shapes of the liquid-liquid interface on the modified surfaces of the channel. The advancing (a) and receding (r) contact angles of oil on the oil side (schematic on the left) and the water on the water side (schematic on the right) are shown based on the values given in Table I. (d) When the system is unstable, the interface between the two fluids periodically sheds droplets near the exit junction where the two fluids are separated. The flow is from left to right, and the flow rate is $Q = 0.1$ ml/min in this case. The light gray fluid is perfluorodecalin (oil), and the dark gray fluid is dyed water-glycerol mixture (water). The geometric parameters of the channel are $H = W = 0.75$ mm, $L_m = 12.5$ mm, $L_e = 30$ mm, and $\alpha = 45°$. (e) The snapshots here show the formation of interfacial bumps in the channels with different lengths: (i) $L_m = 12.7$ mm, (ii) $L_m = 21.4$ mm, and (iii) $L_m = 50.9$ mm. The flow rate in all cases is $Q = 0.1$ ml/min. All scale bars represent 2 mm.

system, none of these studies have investigated the instability itself, leaving its localized nature elusive.

Here, combining experiments, numerical simulations, and global stability analysis, we characterize the instability of parallel two-phase flows in finite channels, showing that the interface between two immiscible fluids flowing at the same rate in a symmetric channel can become locally unstable near the exit junction where the fluids are separated. We find that the straight interface develops a localized "bump," which grows over time and protrudes into the stream of the second fluid and eventually result in drop shedding. The drop shedding behavior is found to be periodic, and the period scales inversely with flow speed. Our numerical simulations qualitatively reproduce the experimental observations and show that the flow can become globally unstable under certain conditions. Finally, balancing the viscous pressure drop along each stream with the Laplace pressure drop across the interface, we obtain a generic stability criterion that agrees well with our experimental observations. The stability criterion is used to deduce quantitative arguments

TABLE I. Table summarizing the various fluids used in the experiments and their properties. The first two fluid pairs have PFD as the oil phase, and the next two have light mineral oil as the oil phase. γ is the interfacial tension of fluid 1 with its respective fluid 2, and θ_r is the receding contact angle of the fluid on its side of the surface modified channel.

Pair	Oil phase	Aqueous phase	ρ [kg/m^3]	μ [mPa s]	γ [mN/m]	θ_r
	PFD		1930	5.6±0.2		<5°
A		50.5% glycerol in water	1126.1	5.7±0.2	43.9±2.9	60.7° ± 2°
B		52% glycerol in water	1130.2	6.1±0.1	43.6±1.7	53.9° ± 4°
	Light mineral oil		838	27.5±0.2		45.8° ± 4°
C		74% glycerol in water	1190	27.6±0.3	28.0±4.0	42.5° ± 5°
D		74.2% glycerol in water	1190	28.5±0.2	24.0±4.3	42.5° ± 5°

that highlight the fact that the stability of the flow system is sensitive to the parameters involved, including the geometry and placement of the exit tubing.

II. EXPERIMENTAL SETUP

We fabricated the microfluidic devices for the experiments using polydimethylsiloxane (PDMS) and a 3D printed (Formlabs Form 2) mold. All the walls of the channels in the device were made of PDMS and were later surface modified. Figure 1(a) shows a schematic of the experimental flow system, and Fig. 1(b) shows a 3D schematic of the typical channel geometry we used in our experiments. The fluids enter via the two inlet channels on the left, flow parallel to each other in the main channel of length $L_m \in [1.5–50]$ mm, and exit via the two channels of length $L_e \in [5–30]$ mm on the right. From the end of the exit channels, polytetrafluoroethylene (PTFE) tubing of inner radius $R_t \in [0.19–0.28]$ mm and length $L_t = 18$ mm carries the fluids to their respective reservoirs. The tip of the exit tubes sits just under the liquid interface in the reservoir to achieve atmospheric pressure p_0 at the exit. The relative height between the PDMS channel and the tip of the exit tubes is defined as h_r [see Fig. 1(a)]. The liquid-liquid interface forms along the length of the main channel and ends at the exit junction where the two liquids are separated. The width of the two inlet and exit channels as well as the half-width of the main channel are all equal $W \in [0.75–1.5]$ mm, and the height of the channels is $H \in [0.3–0.75]$ mm. The angle that the main channel makes with the exit channel is $\alpha \in [0°–90°]$. We selectively modify the wettability of the channel surfaces, using a coflow surface modification procedure, to help achieve a parallel two-phase flow [18] (see Supplemental Material Sec. I [19]). We conducted each experiment immediately after surface modification, and the devices were not reused.

We used four different fluid pairs in the experiments, as summarized in Table I. Fluid pairs A and B had perfluorodecalin (Fluorochem, PFD) as the oil phase and pairs C and D had light mineral oil (Sigma-Aldrich) as the oil phase. All fluid pairs had a glycerol-deionized (DI) water mixture as the aqueous or water phase. The density ρ, viscosity μ, interfacial tension γ, and receding contact angle θ_r after surface modification on that specific fluid's side of the channel are all reported in Table I. Viscosity of the aqueous phase was measured after making the solution and just before the experiments in order to make sure that the hygroscopic nature of glycerol had minimal effect on our results. In all of the experiments, unless otherwise noted, the two fluids were introduced into the device by the same syringe pump (Harvard Apparatus PHD ULTRA) to keep the flow rates equal. The flow rates were varied between 0.005 ml/min and 0.4 ml/min, corresponding to Reynolds numbers in the range of Re $= \rho_2 U H / \mu_2 = O(0.01–1)$, where the fluid properties of the oil phase were used and U is the average flow velocity in the channel. Although the two fluids we use have different densities, the Bond numbers, representing the relative magnitudes of gravitational and surface tension effects, are in the range of Bo $= \Delta \rho g H^2 / \gamma = O(0.01–0.1)$. We observe that the interface between the two fluids remains symmetric with respect to the top and bottom walls.
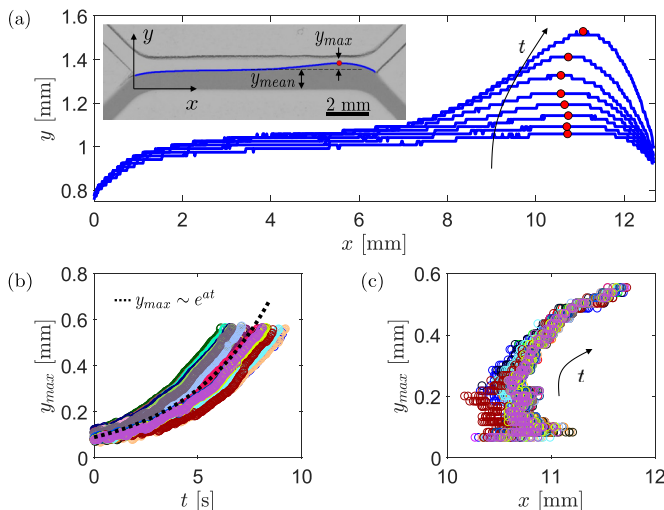
FIG. 2. The spatiotemporal evolution of the unstable interface. (a) A bump, characterized by the length scale y_{max}, develops near the exit junction where the two fluids are being separated. The red dot represents the maximum point on the interface, and the dashed black line in the inset represents the mean interface location y_{mean}. A space-time diagram shows the progression of the interface profile during a drop shedding event. The evolution of the magnitude of y_{max} in time and the horizontal location along the channel where it occurs is tracked in panels (b) and (c), respectively. Different colors represent different drop shedding events within the same experiment at a constant flow rate $Q = 0.1$ ml/min using fluid pair B. The bump approximately follows an exponential growth in this case as shown in (b).

Therefore, inertial and gravitational effects are expected to be small within the channel flow. We will later discuss the importance and the effect of gravity on the stability of the interface when considering the exit tubing.

III. CHARACTERIZATION OF THE INSTABILITY

The instability manifests itself as a periodic growth of an interfacial bump near the exit junction where the two fluids are separated. This bump grows in time and leads to drop shedding as shown in Fig. 1(d). After a drop is pinched off, the interface relaxes back to its original position in the middle of the channel and subsequently grows again. Drop pinch-off in microfluidic junctions is caused by the pressure drop across a growing thread of immiscible liquid and is likely the same cause for pinch-off in our observation [20]. But the focus of this work will be in deciphering the reason behind the growth of the interfacial bump that precedes the drop pinch-off phenomenon.

The choice of the fluid pairs for the experiments and the choice of injecting both fluids at the same flow rate were intentional. The goal was to achieve a perfectly symmetric flow, which turned out to be unfeasible owing to the difficulty in exactly matching the viscosity of two immiscible fluids. So we tried to closely match the viscosity of the oil phases in one of its fluid pairs (pairs A and C in Table I) and intentionally made the second one have a higher viscosity contrast (pairs B and D in Table I). We observed that for a given fluid pair with a certain viscosity contrast, the flow became unstable above a critical flow rate and this critical flow rate decreased with increasing viscosity contrast.

A series of experiments was performed to study the effect of channel geometry on the instability. We varied the length L_m of the middle channel to test whether the instability is convective or absolute [21–23] and observed that the instability is always localized at the exit junction [Fig. 1(e)]. The other geometric features of the channel, including height, width, and exit angle, were also systematically
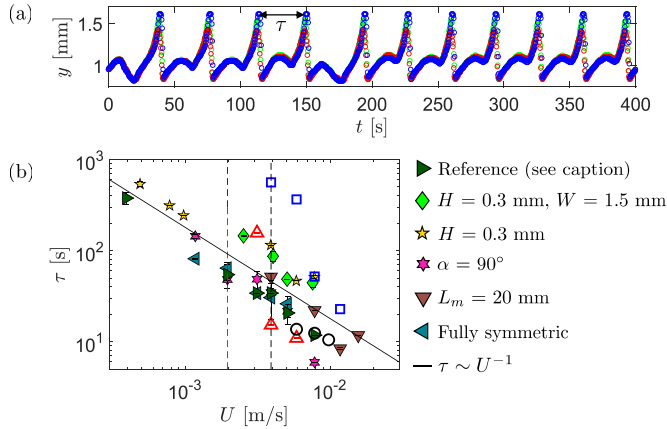
FIG. 3. The drop shedding caused by the instability is periodic in time. (a) The red, green, and blue data points represent the temporal evolution of the height of three different points along the interface near the bump. The bump grows in time until it touches the wall on the opposite side of the channel. A drop is then shed and the interface relaxes, leading to a sudden decrease in the interface location. The interface growth is then repeated periodically in time. (b) The period of the drop shedding decreases as the flow rate increases, showing a scaling $\tau \sim 1/U$. Varying the geometric features of the device affects the period. In the legend the reference geometry corresponds to $H = W = 0.75$ mm, $L_m = 12.5$ mm, $L_e = 30$ mm, and $\alpha = 45°$. All other cases shown in the legend are variations of the reference geometry, where one of the geometric features is changed. Fluid pair A was used for all of the closed data points, and h_r was such that the flow was unstable for all of the flow speeds studied. The open data points correspond to situations where the critical flow speed below which the flow is stable, indicated by the dashed line of the same color, was within the window of flow speeds studied. The blue open squares correspond to fluid pair B with $h_r = 0$ mm, the red open triangles correspond to fluid pair C with $h_r = 0$ mm, and the black open circles correspond to fluid pair D with $h_r = 0$ mm.

varied, and we found that the qualitative behavior of the instability and the evolution of the interface [Fig. 1(d)] are independent of these parameters. However, the critical flow rate above which the flow became unstable for a given fluid pair was found to be a function of the height and width of the channel. Similar instability behavior was observed in a "fully symmetric" configuration where the fluids entered from four inlets on the side and exited via two outlets perpendicular to the main channel in the middle (see the Supplemental Material Fig. 2 [19]). This configuration placed the interfacial stagnation point within the bulk of the fluid instead of at the wall, but seemed to have little effect on the overall stability of the flow. In other words, apart from slightly shifting the critical flow rate above which the flow becomes unstable, the geometric features of the channel did not play a major role in stabilizing or destabilizing the flow system.

To characterize the growth of the instability, we track the evolution of the interface in time. We define the bump height, y_{max}, as the vertical distance between the highest point on the interface and the mean height of the interface, y_{mean}, in the middle of the channel (Fig. 2). The bump grows in time until it touches the opposite wall of the channel while the remainder of the interface in the channel remains nearly fixed in time. The bump growth remains localized near the exit junction with the peaks shown with red dots in Fig. 2(a) having a nearly fixed x coordinate before getting sheared off towards the exit channel at later times [Fig. 2(c)]. The temporal evolution of the bump height y_{max} is shown in Fig. 2(b) for multiple drop shedding events (different colors) within the same experiment for a fixed flow rate of $Q = 0.1$ ml/min. Here, $t = 0$ s is the time at which the bump starts to grow for each drop shedding event.

The temporal evolution of bump height follows an exponential growth [Fig. 2(b)], suggesting a linear instability. However, we note that in most of our experiments the growth of the bump is affected by the previously shed droplet that is still traveling through the tubing and has not

yet reached the exit reservoir. The additional pressure perturbation caused by this traveling drop often interferes with the growth of the bump and typically slows the growth, therefore deviating the evolution from the exponential growth expected in an ideal setting.

The growth of the instability leads to periodic drop shedding. We characterize this periodicity by measuring the dominant frequency and the period by taking the Fourier transform of the time series of several different points along the interface near the bump. This dominant mode represents the period of the drop shedding, τ, as shown in Fig. 3(a). The measured period scales inversely with the average flow velocity, i.e., $\tau \sim 1/U$, where $U = Q/A$ with A as the cross-sectional area of the channel. Therefore, a faster flow leads to a smaller period. Varying the geometric features also affects the period as shown in Fig. 3(b); for practical purposes, a flow was considered "stable" if no drop shedding event took place within 1 h. For the cases where the flow was stable below a critical flow speed within the window of flow speeds considered here, indicated by open symbols in Fig. 3(b), the period seems to reach $\tau \sim 1/U$ behavior as the flow speed is increased away from the critical flow speed.

IV. NUMERICAL RESULTS

A. Simulations

We also conducted a 2D numerical study to better understand the nature of this instability (see the Supplemental Material Secs. III and IV [19,24]). The numerical system had two fluids with a certain viscosity contrast injected at the same flow rate through a symmetric channel and had the same exit pressure, resembling the conditions of the experimental system. The channel geometry and the fluid properties were also comparable to that from experiments (see the Supplemental Material Sec. III E [19]).

The base state interface profiles for three different flow rates, for the case $\mu_2/\mu_1 = 0.92$, is shown in Fig. 4(a). Notice that the interface becomes more deformed near the exit junction with increasing flow rate. For a fixed viscosity ratio between the two fluids, increasing the flow rate increases the difference in viscous pressure drop between the two phases. The higher difference in pressure between the two fluids results in a more deformed interface. The fact that the deformations get localized near the exit junction is a consequence of the interface trying to satisfy the pressure jump condition with the prescribed background flow field in a finite width channel. Out of all the base states shown in Fig. 4(a), only the largest flow rate is unstable. The spatiotemporal evolution of the interface for this unstable case is plotted in Fig. 4(b), where the local growth of the interface, the bump, is clearly visible. Figure 4(c) shows contours of the pressure field in the channel along the length of the interface as the interface becomes unstable. Most of the changes in the pressure field are localized near the exit junction as the interface grows from its already deformed base state; the channel exit, which is further downstream, would be at the imposed identical pressure.

B. Global stability analysis

We study the stability of the base state solutions by calculating the linear 2D global modes and assuming the temporal dependence

$$\Psi(x, y; t) = \Psi_b(x, y) + \epsilon \delta \Psi(x, y) e^{-i\omega t}, \tag{1}$$

where Ψ represents any independent variable, Ψ_b is the base state solution, $\delta\Psi$ is the eigenmode with $\epsilon \ll 1$, and $\omega = \omega_r + i\omega_i$ is the eigenvalue. Figure 4(d) shows the growth rate of the instability, the imaginary part of ω, as a function of flow rate Q. In the presence of a small viscosity difference between the two fluids, the flow becomes globally unstable beyond a critical flow rate, and this instability prevents perfect separation of the two fluids at the exit junction. Our numerical simulations and stability analysis qualitatively reproduce the instability observed in the experiments, but cannot be quantitative since the simulations are 2D and leave out the dynamics of the 3D interface.
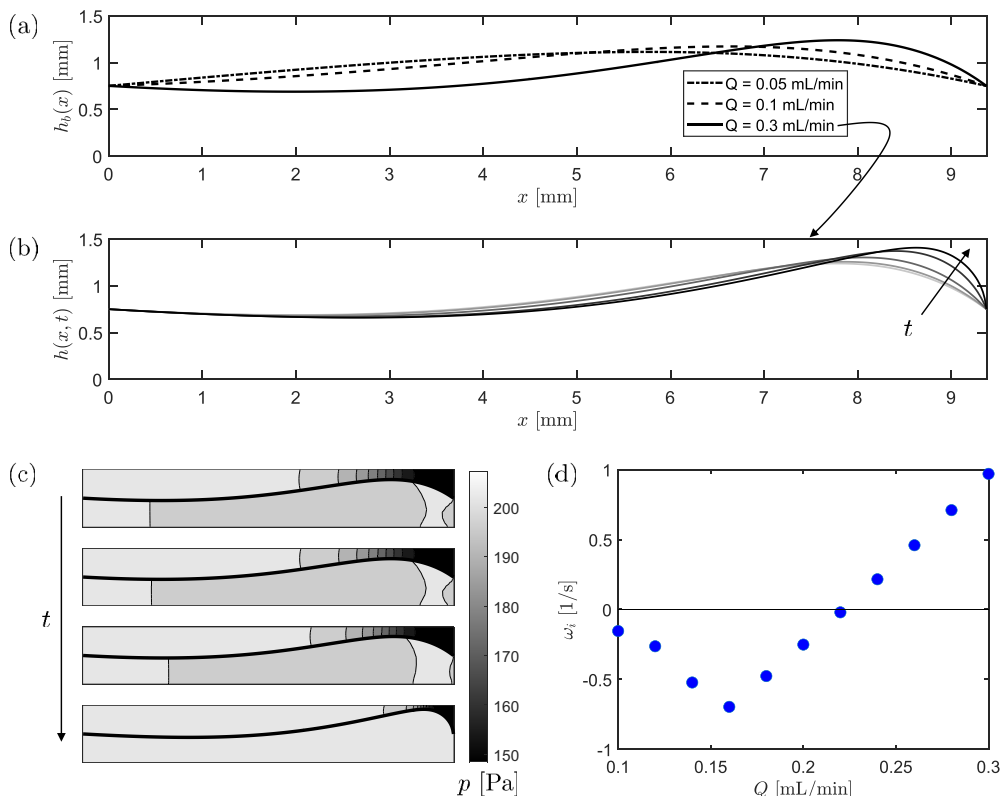
FIG. 4. Results from our numerical study with two fluids of viscosity ratio $\mu_2/\mu_1 = 0.92$. Fluid 1 is below the interface, and fluid 2 is above the interface. Fluid properties used for this simulation are as follows: $\mu_1 = 5.6$ mPa s, $\rho_1 = 1124$ kg/m^3, $\rho_2 = 1930$ kg/m^3, and $\gamma = 37.0$ mN/m. (a) Base (steady) state interface profiles for three different flow rates. Only the largest flow rate, $Q = 0.3$ ml/min, is unstable. (b) Spatiotemporal evolution of the interface for the unstable case $Q = 0.3$ ml/min showing the interface deforming more from its base state over time. The local growth of the interface near the exit junction is similar to that seen in experiments. (c) Evolution of the pressure field in the channel as the interface deforms and becomes unstable for the case with $Q = 0.3$ ml/min. The solid black line is the interface. Note that most of the changes occur locally near the exit junction. (d) The growth rate ω_i of the linear instability as a function of flow rate. The flow is globally unstable when $\omega_i > 0$.

V. MECHANISM OF THE INSTABILITY

The instability observed in the experiments, the numerical simulations, and stability analysis can be explained using a pressure argument. We expect the liquid-liquid interface to be stable as long as the contact angle remains between its measured static advancing and receding values [Fig. 1(c)]. The bounds on the contact angle translate to upper and lower bounds on the pressure difference across the interface via the Laplace pressure jump condition,

$$\frac{-2\gamma \cos \theta_{r,1}}{H} < p_1 - p_2 < \frac{2\gamma \cos \theta_{r,2}}{H}, \tag{2}$$

in which $\theta_{r,1}$ is the receding contact angle of fluid 1 on its side of the channel and $\theta_{r,2}$ is the receding contact angle of fluid 2 on its side of the channel [Fig. 1(c)]. To reduce confusion, we will always label the invading fluid to be fluid 1 and therefore have to consider only an upper limit on the Laplace pressure jump condition.
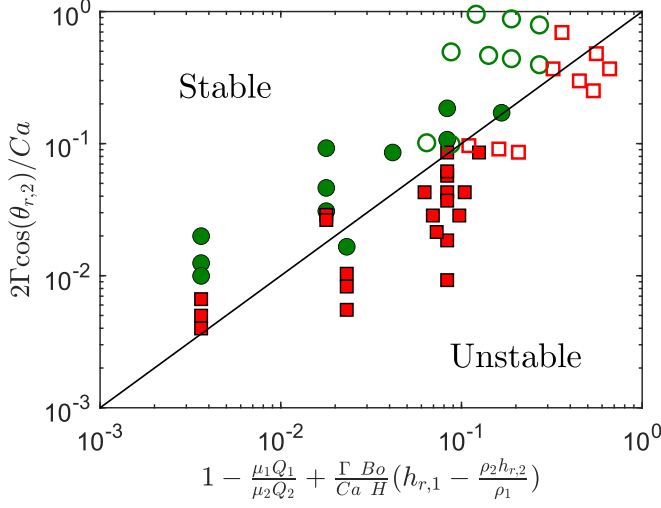
FIG. 5. Instability phase diagram for the parallel two-phase flow. The closed data points are from our experiments with all four fluid pairs, and the open data points are from the literature [17]. The invading fluid (fluid 1) is always water in our experiments, and it is oil in the data from [17]. The solid line represents the stability criterion [Eq. (5)]. Here unstable (red squares) corresponds to imperfect separation of the two fluids, and stable (green circles) corresponds to perfect separation.

The pressure on either side of the interface depends on the viscous pressure drop through each phase, which has contributions from flow through the PDMS exit channel and the exit tubing, and the hydrostatic pressure from the relative height h_r between the channel and the tip of the exit tube. The pressure drop from one side of the interface at the exit junction to the reservoir can be written as

$$p_i - p_0 = \left(\frac{\mu_i Q_i L}{kA}\right)_e + \left(\frac{\mu_i Q_i L}{kA}\right)_t + \rho_i g h_{r,i}, \tag{3}$$

where k is the permeability, i.e., a geometric quantity that enters the description of the hydrodynamic channel-flow resistance, subscript "e" corresponds to the exit channel, "t" corresponds to tube, and $i = 1, 2$ represent fluids 1 and 2, respectively. Taking the difference between the viscous pressure drops in the two phases for the most general case, we arrive at

$$p_1 - p_2 = (\mu_1 Q_1 - \mu_2 Q_2)\left[\left(\frac{L}{kA}\right)_e + \left(\frac{L}{kA}\right)_t\right] + g(\rho_1 h_{r,1} - \rho_2 h_{r,2}). \tag{4}$$

Here $p_1 - p_2$ is bounded by equation (2) where we take the upper bound to be the critical capillary pressure Δp_c. For the flow to be unstable, $p_1 - p_2 > \Delta p_c$ where $\Delta p_c = 2\gamma (\cos\theta)/H$. Since the invading fluid is labeled as fluid 1, the θ in Δp_c is the receding contact angle of fluid 2 on its side of the channel, namely, $\theta_{r,2}$. Applying this condition and rearranging the terms, we arrive at a dimensionless inequality that must be met for the instability to occur,

$$1 - \frac{\mu_2 Q_2}{\mu_1 Q_1} + \frac{\Gamma \, \text{Bo}}{\text{Ca} \, H}\left(h_{r,1} - \frac{\rho_2 h_{r,2}}{\rho_1}\right) > \frac{2\Gamma \cos(\theta_{r,2})}{\text{Ca}}, \tag{5}$$

where $\text{Ca} = \mu_1 U_1/\gamma$ is the capillary number, $\text{Bo} = \rho_1 g H^2/\gamma$ is the Bond number, and $\Gamma = [H^3(\frac{12L_e}{H^4} + \frac{8L_t}{\pi R_t^4})]^{-1}$ is a dimensionless resistance through the flow system. Here, we use the permeabilities $k_e = H^2/12$ and $k_t = R_t^2/8$. Based on this instability criterion, all of our experimental observations can be mapped onto a phase diagram that is shown in Fig. 5. The theoretical prediction agrees reasonably well with our observations, and the discrepancies can be attributed to extra

sources of dissipation in the real system, such as adhered droplets and thin films along the channel and the tube-to-PDMS connections. In Fig. 5 we also include some of the data from the literature [17] (open data points), which further confirm the validity of our instability criterion across various experimental conditions.

A direct consequence of the mechanism of the instability is that even small differences in viscosity between the two fluids can lead to instability under certain conditions. Considering that the two fluids are injected at the same flow rate Q and that $h_{r,1} = h_{r,2} = 0$, the criterion for instability becomes $\Delta\mathrm{Ca} > 2\Gamma\cos(\theta_{r,2})$ where $\Delta\mathrm{Ca} = (\mu_1 - \mu_2)U_1/\gamma$. Here the critical capillary number beyond which the flow becomes unstable is only a function of geometrical parameters of the system and the contact angle. An analogous stability criteria is derived in the Supplemental Material for the 2D case explored in the simulations (see the Supplemental Material Sec. IV C [19]) to show that the results from the simulations can also be explained by this instability mechanism. Note that the instability here arises as a result of the finite nature of the flow system amplifying the asymmetry introduced by the viscosity contrast, whereas viscous stratification alone can be responsible for an instability in infinite two-phase flows [10]. The modified criterion predicts that even a moderate viscosity difference of 0.1 mPa s will lead to an unstable flow in our system with fluid pair C when the flow rate is approximately above 0.1 ml/min (Re ≈ 0.8) which is in agreement with our experiments. Additionally, if the two fluids have different densities, the flow could become unstable when either $h_{r,1}$ or $h_{r,2}$ is nonzero and finite even if the fluids have exactly the same viscosity. Considering the properties of our fluid pair A with $\mu_1 = \mu_2$, $Q_1 = Q_2$, and $h_{r,1} = 0$, the flow will be unstable independent of the value of the flow rate as long as $h_{r,2} < -5$ mm, i.e., more than 5 mm below the level of the PDMS device. These scenarios highlight the fact that the stability of this parallel two-phase flow is extremely sensitive to the various parameters in the flow system.

VI. CONCLUSION

The symmetry breaking of a parallel two-phase flow in a finite channel manifested itself as an instability that prevented complete separation of the two fluids. Our experiments and numerical simulations showed that this instability always takes place near the exit junction of the channel where an interfacial bump forms and results in drop shedding. The drop shedding behavior was found to be periodic in nature, and the period scales as $\tau \sim 1/U$. The instability occurs when the mismatch in viscous pressure drop along the two phases exceeds a critical Laplace pressure jump. Even small differences in viscosity between the two fluids can lead to an instability if the injected flow rates are high enough. In the future, a complete theoretical analysis could be done at the exit junction of the interface to further understand the growth of the instability. Nevertheless, the discussed stability criterion and the sensitive nature of the instability will serve as important guidelines for controlling parallel two-phase flows, thereby making it more tractable for applications.

---

[1] J. Burns and C. Ramshaw, Development of a microreactor for chemical production, Chem. Eng. Res. Des. **77**, 206 (1999).

[2] D. A. Wenn, J. E. Shaw, and B. Mackenzie, A mesh microcontactor for 2-phase reactions, Lab Chip **3**, 180 (2003).

[3] T. Maruyama, J.-I. Uchida, T. Ohkawa, T. Futami, K. Katayama, K.-I. Nishizawa, K.-I. Sotowa, F. Kubota, N. Kamiya, and M. Goto, Enzymatic degradation of p-chlorophenol in a two-phase flow microchannel system, Lab Chip **3**, 308 (2003).

[4] S.-X. Meng, L.-H. Xue, C.-Y. Xie, R.-X. Bai, X. Yang, Z.-P. Qiu, T. Guo, Y.-L. Wang, and T. Meng, Enhanced enzymatic reaction by aqueous two-phase systems using parallel-laminar flow in a double Y-branched microfluidic device, Chem. Eng. J. **335**, 392 (2018).

[5] P. F. Jahromi, J. Karimi-Sabet, and Y. Amini, Ion-pair extraction-reaction of calcium using Y-shaped microfluidic junctions: An optimized separation approach, Chem. Eng. J. **334**, 2603 (2018).

[6] I. Robins, J. Shaw, B. Miller, C. Turner, and M. Harper, Solute transfer by liquid/liquid exchange without mixing in micro-contactor devices, in *Microreaction Technology*, edited by W. Ehrfeld (Springer, 1998), pp. 35–46.

[7] M. Surmeian, M. N. Slyadnev, H. Hisamoto, A. Hibara, K. Uchiyama, and T. Kitamori, Three-layer flow membrane system on a microchip for investigation of molecular transport, Anal. Chem. **74**, 2014 (2002).

[8] T. Maruyama, H. Matsushita, J.-I. Uchida, F. Kubota, N. Kamiya, and M. Goto, Liquid membrane operations in a microfluidic device for selective separation of metal ions, Anal. Chem. **76**, 4495 (2004).

[9] U. Novak, A. Pohar, I. Plazl, and P. Žnidaršič-Plazl, Ionic liquid-based aqueous two-phase extraction within a microchannel system, Sep. Purif. Technol. **97**, 172 (2012).

[10] C.-S. Yih, Instability due to viscosity stratification, J. Fluid Mech. **27**, 337 (1967).

[11] R. Dreyfus, P. Tabeling, and H. Willaime, Ordered and Disordered Patterns in Two-Phase Flows in Microchannels, Phys. Rev. Lett. **90**, 144505 (2003).

[12] P. Guillot and A. Colin, Stability of parallel flows in a microchannel after a T junction, Phys. Rev. E **72**, 066301 (2005).

[13] A. Hibara, M. Nonaka, H. Hisamoto, K. Uchiyama, Y. Kikutani, M. Tokeshi, and T. Kitamori, Stabilization of liquid interface and control of two-phase confluence and separation in glass microchips by utilizing octadecylsilane modification of microchannels, Anal. Chem. **74**, 1724 (2002).

[14] A. Aota, A. Hibara, and T. Kitamori, Pressure balance at the liquid-liquid interface of micro countercurrent flows in microchips, Anal. Chem. **79**, 3919 (2007).

[15] A. Aota, K. Mawatari, S. Takahashi, T. Matsumoto, K. Kanda, R. Anraku, A. Hibara, M. Tokeshi, and T. Kitamori, Phase separation of gas–liquid and liquid–liquid microflows in microchips, Microchim. Acta **164**, 249 (2009).

[16] D. Ciceri, J. M. Perera, and G. W. Stevens, The use of microfluidic devices in solvent extraction, J. Chem. Technol. Biotechnol. **89**, 771 (2014).

[17] P. F. Jahromi, J. Karimi-Sabet, Y. Amini, and H. Fadaei, Pressure-driven liquid-liquid separation in Y-shaped microfluidic junctions, Chem. Eng. J. **328**, 1075 (2017).

[18] B. Zhao, J. S. Moore, and D. J. Beebe, Surface-directed liquid flow inside microchannels, Science **291**, 1023 (2001).

[19] See Supplemental Material at http://link.aps.org/supplemental/10.1103/PhysRevFluids.7.033904 for details about surface modification and numerical simulations.

[20] P. Garstecki, M. J. Fuerstman, H. A. Stone, and G. M. Whitesides, Formation of droplets and bubbles in a microfluidic T-junction—Scaling and mechanism of break-up, Lab Chip **6**, 437 (2006).

[21] P. Huerre and P. A. Monkewitz, Local and global instabilities in spatially developing flows, Annu. Rev. Fluid Mech. **22**, 473 (1990).

[22] J.-M. Chomaz, Global instabilities in spatially developing flows: Non-normality and nonlinearity, Annu. Rev. Fluid Mech. **37**, 357 (2005).

[23] C. Duprat, C. Ruyer-Quil, S. Kalliadasis, and F. Giorgiutti-Dauphiné, Absolute and Convective Instabilities of a Viscous Film Flowing Down a Vertical Fiber, Phys. Rev. Lett. **98**, 244502 (2007).

[24] M. Herrada and J. Montanero, A numerical method to study the dynamics of capillary fluid systems, J. Comput. Phys. **306**, 137 (2016).